SCIENCE CHINA
Technological Sciences

doi: 10.1007/s11431-012-4777-x

Bioelectrochemical control mechanism with variable-frequency regulation for skeletal muscle contraction—Biomechanics of skeletal muscle based on the working mechanism of myosin motors (II)

YIN YueHong* & CHEN Xing

State Key Laboratory of Mechanical System and Vibration, Institute of Robotics, Shanghai Jiao Tong University, Shanghai 200240, China

Received August 24, 2011; accepted December 26, 2011

This paper presents a bioelectrochemical model for the activation of action potentials on sarcolemma and variation of Ca^{2+} concentration in sarcomeres of skeletal muscle fibers. The control mechanism of muscle contraction generated by collective motion of molecular motors is elucidated from the perspective of variable-frequency regulation, and action potential with variable frequency is proposed as the control signal to directly regulate Ca^{2+} concentration and indirectly control isometric tension. Furthermore, the transfer function between stimulation frequency and Ca^{2+} concentration is deduced, and the frequency domain properties of muscle contraction are analyzed. Moreover the conception of "electro-muscular time constant" is defined to denote the minimum delay time from electric stimulation to muscle contraction. Finally, the experimental research aiming at the relation between tension and stimulation frequency of action potential is implemented to verify the proposed variable-frequency control mechanism, whose effectiveness is proved by good consistence between experimental and theoretical results.

molecular motor, muscle fiber, action potential, Ca^{2+} concentration, regulation mechanism

Citation: Yin Y H, Chen X. Bioelectrochemical control mechanism with variable-frequency regulation for skeletal muscle contraction—Biomechanics of skeletal muscle based on the working mechanism of myosin motors (II). Sci China Tech Sci, 2012, doi: 10.1007/s11431-012-4777-x

1 Introduction

Great progress has been made on the research of macroscopic contraction properties of skeletal muscle since the proposal of Hill model [1], and the measurement and model for mechanical features of muscle are becoming more elaborate [2–5]. The macroscopic contraction properties of muscle can be studied through isometric tension and isotonic tension, in which the measured physical quantities include sarcomere length, tension, contraction distance, contraction speed, and so on. The coupled relations between these quantities form the dynamical characteristics of muscle contraction. On the other hand, Huxley made important contributions to the revelation of microscopic mechanism of muscle contraction [6, 7] and proposed the famous sliding filament theory [8]. The microscopic research of skeletal muscle is mainly based on in vitro experiments, the scales can be muscle fiber, sarcomere, thick/thin filament or single molecule. The advantages of in vitro microscopic experiments are that cytoplasm environment of the objective tissue including solution components can be adjusted manually, and information like membrane potential and concentrations of all kinds of ions can be obtained besides physical quantities like tension and displacement, so that the factors

*Corresponding author (email: yhyin@sjtu.edu.cn)

affecting muscle contraction can be identified. These researches have shown that ATP and Ca^{2+} are essential to muscle contraction [9], for the reason that the formation of cross bridges needs the exposure of corresponding sites for myosin binding on thin filaments, while the exposure is initiated by Ca^{2+} binding to troponin on thin filaments. In order to do work, myosin needs to consume the energy produced by ATP hydrolysis. Thus, on microscopic scale, the corresponding concentrations—[ATP] and [Ca^{2+}]—directly affect the stochastic characteristics of collective motor motion, which decides the muscle power. Furthermore, [ATP] is nearly constant during normal operation process of muscle, so the variation of [Ca^{2+}] characterizes the drive signal of muscle. Correspondingly, action potentials on muscle fiber represent the control signal because they dominate the start and stop of Ca^{2+} release.

As mentioned above, the understanding of macroscopic and microscopic mechanism of muscle contraction has become clearer, and physical explanation has also been provided toward how the control signal-like action potentials transform into drive signal [10]. While there have been plenty of studies revealing the relationship between [Ca^{2+}] and tension or stimulation rate of action potential and tension, the correlation between wave characteristics of action potential and [Ca^{2+}] variation remains unclear, i.e., the understanding of the control principium of how the control signal modulates the drive signal is still not complete. Due to the above problem, there are difficulties in the description of harmonic work of massive muscle fibers, as well as how motion intention is realized. Therefore, elucidating this regulation mechanism is closely related to the unification of the microscopic and macroscopic skeletal muscle dynamics. Cannell and Allen once modeled and calculated the Ca^{2+} movements in sarcomeres [11], with the aim of describing the features of how [Ca^{2+}] gradients change with time and estimating the measurement error of Ca^{2+} indicator. However, they did not exploit the significance of the model from the perspective of control theory. On the other hand, due to the limit of computing technologies at that time and lack of knowledge about sarcomere structures, the simulation results of the model were not so satisfactory. Most studies on the relation between action potential frequency and sarcomere tension were based on experiments, including studies on mammalian cardiac muscle fibers [12]. These works did not extract refined theoretical model or focus on control theory, as a result, there was no strong correlation between the above studies and motion control of muscle. To solve these problems, this paper aims at building a complete bioelectrochemical model describing action potential, the release of Ca^{2+} and the diffusion of [Ca^{2+}], based on the physiologic structures of skeletal muscle fibers. It further discusses the mode and features of the control signal regulating the drive signal so as to indirectly provide the description of how action potentials control muscle tension and verify the stochastic model of collective operation of molecular motor proposed in the preceding paper [13].

2 Modeling of action potentials on sarcolemma

It can be seen from the process of muscle contraction that the action potentials of motor neurons induce new ones on sarcolemma through the neuromuscular junction, and these action potentials characterize the control signal. As shown in Figure 1, a muscle fiber is composed of about 2000 myofibrils (only one is presented here), and each of them is wrapped by sarcoplasmic reticulum (SR), on which there exists periodic tissue called transverse tubule (T-tubule). For mammals, each sarcomere has two T-tubules located at the intersections of A-band and I-band [14]. T-tubules periodically extend to the openings on sarcolemma, thus they are actually filled with extracellular fluid. As a result, T-tubules can transmit action potentials on sarcolemma deeply into myofibrils in a muscle fiber, so that the whole muscle fiber can be excited. On both sides of a T-tubule there are inflated parts called terminal cisterna, which is connected to T-tubule via massive voltage sensitive Ca^{2+} channels (DHPR) [15] and ryanodine channels (RYR) [16], so once T-tubules feel action potentials, the Ca^{2+} channels will immediately open to allow Ca^{2+} of high concentration in terminal cisterna to diffuse into the sarcomere and Ca^{2+} will bind to troponin on thin filaments in order to start the working cycle of molecular motors. There also exist important proteins called Ca-ATP enzyme on terminal cisterna [17]. These enzymes are actually highly efficient Ca^{2+} pumps which recycle the Ca^{2+} back to terminal cisterna, and make the [Ca^{2+}] rapidly decrease to the resting level when stimulations end. Although other types of Ca^{2+} pumps also exist on sarcolemma, Ca-ATP enzymes dominate during the normal work of muscle.

The resting potential of sarcolemma is ~ –85 mV, and the threshold for Na^+ channel to open is 14 mV higher than that. The peak value of action potential is ~ 39 mV [18], and its conduction speed along muscle fibers is ~ 4 m/s, while the radial speed from the surface of a muscle fiber to its

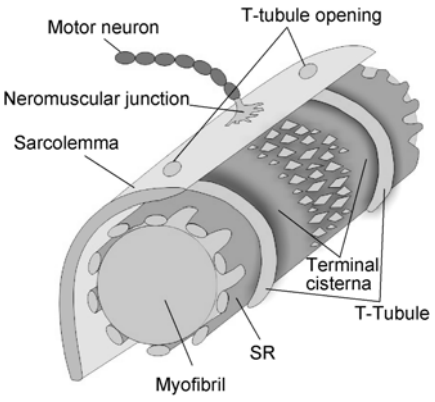

Figure 1 The structure of a muscle fiber.

center is about several centimeters per second [19]. Consequently, the excitations of sarcomeres in different myofibrils are not synchronized, and in order to obtain the drive properties of a single sarcomere, we take the myofibril closest to sarcolemma as the modeling object. The purpose of the model is to get the mathematical description of the action potential shape on sarcolemma and facilitate the investigation of its influence on [Ca^{2+}], as the duration of single action potential directly affects the open interval of Ca^{2+} channels on SR. Na^+ currents coming into the membrane and K^+ currents going out of it forms the physical basis of sarcolemma electric activities, which are governed by the open and close of Na^+ channels and K^+ channels, while the instantaneous potential of sarcolemma is decided by the charge density (concentrations of different types of ions) inside and outside of it. It should be noted that voltage sensitive Na^+ channels distribute on sarcolemma while most voltage sensitive K^+ channels are located at T-tubules. According to such distribution features of channels, we can flatten the sarcolemma and the cylindrical muscle fiber in Figure 1, and select the cytoplasm between neighboring T-tubules (also between sarcolemma and SR) as the modeling region, as shown in Figure 2. With general sense, we take the central point of this region as the ion concentration reference point inside the membrane (ion concentrations outside are approximately constant), i.e., the membrane potentials on sarcolemma can be characterized by the potentials at the central points between successive T-tubules. Once action potentials arrive at these points, the membrane potential will immediately jump to the peak value, while its decrease rate is decided by the speed of K^+ diffusing out of the membrane, and this is related to the K^+ channel density on T-tubules, i.e., the higher the density, the faster the diffusion. During the analysis we use the area ratio of total K^+ channel opening to the wall of T-tubule per unit area to represent the K^+ channel density, and denote it as η_K. The K^+ channels on T-tubules will rapidly open when they feel potential rise. During the out flowing of K^+, they will firstly fill into T-tubules, and then diffuse to extracellular regions through the T-tubule openings on sarcolemma, i.e., the decrease rate of [K^+] in cytoplasm is determined by the diffusion speed of K^+ at the openings. We set [K^+] as n_K, and the

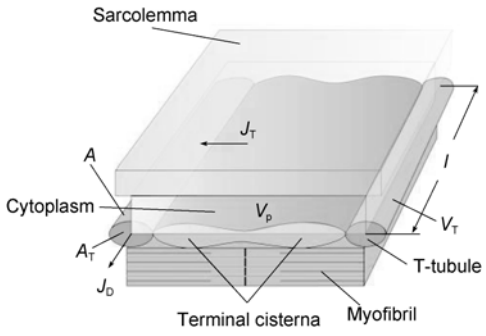

Figure 2 [K^+] calculation model of the cytoplasm near sarcolemma.

K^+ current from cytoplasm to T-tubule as J_T, thus from diffusion dynamics we know that J_T can be described by the concentration gradient at the T-tubule wall:

$$J_T = -D_K \frac{\partial n_K}{\partial r}, \tag{1}$$

where D_K is the diffusion coefficient of K^+, and $D_K = \mu k_B T$, where μ is the drift speed of the considered particle and $\mu = \tau/m_k$, in which τ denotes the average time interval between successive particle collisions during Brownian motion. Under mammalian body temperature, the mean free path of a particle can be approximately regarded as of the order of Å; with the theorem of energy equipartition we can get τ= ~1.8×10^{-13} s. The mass of K^+ is denoted by m_k, and m_k = ~6.477×10^{-26} kg, while k_B = 1.38×10^{-23} J/K, being the Boltzman constant. We take T = 310.15 K as the human body temperature. Finally, we get D_K = ~1.196×10^{-8}. The r in eq. (1) represents the radial direction of a T-tubule, inside of which the change of [K^+] with time can be written as

$$\frac{\partial n_K}{\partial t} = -J_T \frac{\eta_K A}{V_T}, \tag{2}$$

where A is the total area of the wall of a T-tubule, whose volume is V_T. With eq. (2), [K^+] becomes

$$n_K = \frac{\eta_K A}{V_T}\left|J_T\right| t + \text{Const.} \tag{3}$$

It can be seen from eq. (3) that n_K is proportional to η_K at the same radial position of a T-tubule and the same time. On the other hand, the loss rate of K^+ in the cytoplasm is decided by the diffusion speed at T-tubule openings, it is still related to the [K^+] gradient at the opening. Consequently, the higher the [K^+] in a T-tubule, the larger the gradient at the opening, i.e., the [K^+] gradient is also proportional to η_K. The diffusion flux of K^+ at the opening is

$$J_D = -D_K \left.\frac{\partial n_K}{\partial x}\right|_{x=l_T}, \tag{4}$$

where x denotes the tangential direction of a T-tubule, whose perimeter is represented by l_T. It has been mentioned that T-tubules wrap around the myofibril, whose diameter is ~1–2 μm. If taking it as 1.5 μm, we get l_T = ~4.712 μm. Accordingly, the variation of [K^+] in cytoplasm can be written as

$$\frac{\partial n_K}{\partial t} = -J_D \frac{A_T}{V_p} = -J_D \frac{1}{L}, \tag{5}$$

where A_T is the cross section area of T-tubule, based on whose physiological geometric parameters the value of A_T is calculated [14]. For the reason that the area can be approximated by a rectangle of 125 nm by 25 nm, A_T = ~ 3.1×10^{-3} μm^2. V_p denotes the cytoplasm volume of the re-

gion shown in Figure 2. The distance between neighboring T-tubules is about half of the length of a sarcomere [2], so we take it as 1 μm, and due to the less than 3 nm layer between sarcolemma and SR, we can set it as 2.5 nm, thus V_p = ~ 11.78×10^{-3} μm^3. $L = V_p/A_T$, which is an effective length, and it is easy to get L = 3.78 μm. Based on the properties of diffusion dynamics and the proportional relation between concentration gradient and η_K mentioned above, we can assume that the gradient in eq. (4) decreases with time exponentially, i.e.,

$$\left.\frac{\partial n_K}{\partial x}\right|_{x=l_T} = -\eta_K a_1 \exp(-b_1 t), \tag{6}$$

where both a_1 and b_1 are undetermined parameters, and a_1 is constant and $a_1 > 0$, meanwhile the decrease coefficient $b_1 > 0$. Substituting eq. (6) into eq. (5) and integrating it, we get the expression of [K^+] in cytoplasm as

$$n_K = \frac{D_K \eta_K a_1}{L b_1}\exp(-b_1 t) + \text{Const.} \tag{7}$$

The [K^+] inside and outside the sarcolemma are 160 mmol/L and 4 mmol/L, respectively [20], therefore when t approaches infinity in eq. (7) n_K should be 4 mmol/L, from which we get Const. = 4 mmol/L. When t = 0, $D_K\eta_K a_1/(Lb_1)$ = 156, and because D_K, a_1 and L are all constants, the decrease coefficient b_1 gains with η_K. Besides, when t = 0 and η_K = 1, the [K^+] gradient should be at maximum, and if denoting it as S_0, we obtain $a_1 = |S_0| = 156/\lambda$, in which λ is the decay length (passing through this length, [K^+] decreases to the value outside from that inside). On the other hand, because the value of membrane potential is decided by the potential difference between inside and outside the membrane, it can actually be regarded as proportional to the effective positive ion concentration difference:

$$E_m = \eta_E(\Delta[Na^+] + \Delta[K^+] + E_r), \tag{8}$$

where E_m is membrane potential with the unit of mV, and η_E is a proportion constant. With the calibration of the relation between the resting potential and [Na^+], [K^+] inside and outside the membrane, we get η_E = ~1. Δ[Na^+] and Δ[K^+] are [Na^+] change and [K^+] change inside the membrane, with the unit of mmol/L. For sarcolemma, the resting [Na^+] inside is ~10 mmol/L [20], and it increases to 135 mmol/L when action potentials happen, so Δ[Na^+] = 125 mmol/L while Δ[K^+] = n_K–160 mmol/L. E_r is the resting potential of the sarcolemma (–85 mV). During the simulation of the action potential we take λ = 1 μm, thus the action potential shapes when η_K changes from 0.1 to 0.5 can be obtained, as shown in Figure 3, from which we can see that the larger the channel density, the faster the action potential decreases, and with η_K approaching 1, the action potential shape converges. As mentioned previously, we know that the K^+ channel density is very high on T-tubules, so η_K can be regarded as 0.5. If we assume that the open condition for Ca^{2+} channels on SR is that the membrane potential is higher than the threshold for action potentials to happen (–71 mV, the horizontal line in Figure 3), it is apparent that the duration of Ca^{2+} channel opening is directly related to that of action potential, due to the very slow deactivation of Ca^{2+} channels. For our situation where η_K = 0.5, this time interval is ~1.8 ms, and the shape of the action potential can be fitted as

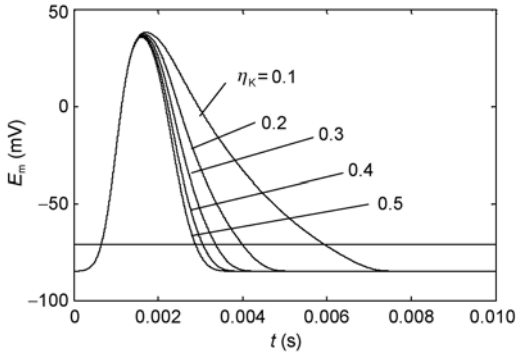

Figure 3 Action potential shapes under different K^+ channel densities.

$$E_{AP} = \frac{t}{a_2}\exp(-t/b_2) + c_2, \tag{9}$$

where $a_2 = 1.569\times10^{-6}$, $b_2 = 5.016\times10^{-4}$, and c_2 = –85. Eq. (9) describes the dynamical feature of a single action potential at a certain point on sarcolemma.

3 [Ca^{2+}] variation inside sarcomeres caused by action potential

If we consider a single sarcomere, it is very small compared with the longitudinal and radial conduction speed of action potentials, thus the conduction time of them on T-tubules can be neglected, and it can be considered that almost all the Ca^{2+} channels on SR will open only if the membrane potential is higher than their open threshold. The [Ca^{2+}] in sarcomeres at resting state is ~10^{-4} mmol/L, and it can be 100 times higher up to 10^{-2} mmol/L, when stimulated [21]. The [Ca^{2+}] on the surface of an excited sarcomere can be regarded as 10^{-2} mmol/L for the reason that sarcomeres are tightly wrapped by SR (Figure 1). Moreover, sarcomere contraction is closely related to the [Ca^{2+}] inside of it, thereby after the sudden rise of [Ca^{2+}] at sarcomere surface, we have to further consider the time needed for this concentration to diffuse deeply into the sarcomere and get uniform. We denote this time as τ_c.

The chemical diffusion process of [Ca^{2+}] can be modeled according to the geometric features of sarcomeres. As shown in Figure 1, sarcomeres are cylindrical, and terminal

cisterna is located between successive T-tubules. Considering that myofibril is composed of periodically patterned sarcomeres, only the part between the T-tubules of a sarcomere (half sarcomere) needs to be investigated, as shown in Figure 4(a). Ca^{2+} channels and Ca^{2+} pumps concentrate on the terminal cisterna [22], while SR distributes sparsely at the central region of a sarcomere, thus we can take 1/3 of the cylinder at both ends in Figure 4(a) as the regions where Ca^{2+} comes in and out. Furthermore, actually we do not have to calculate the concentration change in the whole volume, due to the symmetric characteristics of the cylinder, the boundary condition and initial condition at its wall. No current exists at the ϕ direction, so the calculation of concentration change can be carried out with a cross section passing through the cylinder axis, as shown in Figure 4(b). The diffusion equation of $[Ca^{2+}]$ is

$$\frac{\partial n_{Ca}}{\partial t} = \nabla^2 (D_{Ca} n_{Ca}), \tag{10}$$

where n_{Ca} denotes $[Ca^{2+}]$, and D_{Ca} is the diffusion coefficient, the calculation of which is similar to D_K, and D_{Ca} = ~1.177×10^{-8}. The simulation results show that the $[Ca^{2+}]$ inside the sarcomere gets uniform after at least 0.6 ms, which implies that τ_c = 0.6 ms, as shown in Figure 5(a). Figure 5(b) shows the distribution of $[Ca^{2+}]$ in the sarcomere schematically, and the depth of the yellow color represents the corresponding $[Ca^{2+}]$ value. This implies that the delay time for $[Ca^{2+}]$ in a sarcomere to reach the peak value (10^{-2} mmol/L) from the resting value is τ_c, which is also the time for a sarcomere to be completely stimulated. Besides, the lasting time of the peak value is related to the duration of action potentials, as has been discussed, this time is about 1.8 ms.

The efficiency of Ca^{2+} pumps should be identified when investigating the decrease features of $[Ca^{2+}]$. From physiological data, 20 Ca^{2+} can be delivered by a pump every second, and nearly 90% of the SR surface is occupied by Ca-ATP enzymes, thus given the area of a single pump on SR and the total area of Ca^{2+} exchange region (Figure 4(a)), we can get the total Ca^{2+} current pumped back into SR as

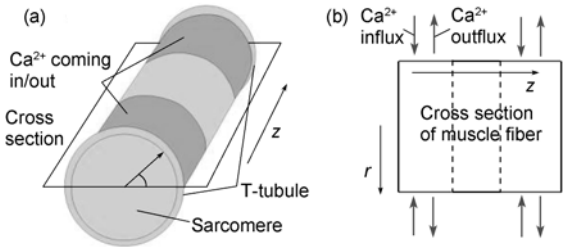

Figure 4 (a) The model of calculation region of $[Ca^{2+}]$; (b) the cross section for calculating $[Ca^{2+}]$.

$$I_{Ca} = \frac{0.9A_c}{A_0} \times 20, \tag{11}$$

where A_c is the area of Ca^{2+} exchange, whose value is ~ 3.1414×10^{-12} m^2 due to the geometric feature of sarcomere. A_0 is the area of a single pump, which can be approximated by a circle with the diameter of 4 nm [23], so A_0 = 1.2567×10^{-17} m^2, and I_{Ca} = 7.4744×10^{-18} mol/s. At the end of action potentials, Ca^{2+} channels are closed, and the Ca^{2+} out flux produced by Ca^{2+} pumps will dominate, therefore the $[Ca^{2+}]$ in a sarcomere can be described by the following continuity equation:

$$\frac{\partial n_{Ca}}{\partial t} = -\frac{I_{Ca}}{V_s}, \tag{12}$$

where V_s characterizes the volume of the cylinder in Figure 4(a), and V_s = 1.7671×10^{-18} m^3. From eq. (12) it can be seen that it costs ~ 2.3 ms for $[Ca^{2+}]$ to drop back to the resting value from the peak value. Based on the above discussion, the $[Ca^{2+}]$ variation process caused by a single action potential can be obtained, as shown in Figure 6, and it can be fitted with the following function:

$$n_{Ca} = \frac{t}{a_3}\exp(-t/b_3) + c_3, \tag{13}$$

where $a_3 = 0.0422$, $b_3 = 0.00121$, and $c_3 = 1\times10^{-4}$. From Figure 6 we see that the shape of n_{Ca} is very similar to that of an action potential, and n_{Ca} approximately follows it, with the delay time of τ_c.

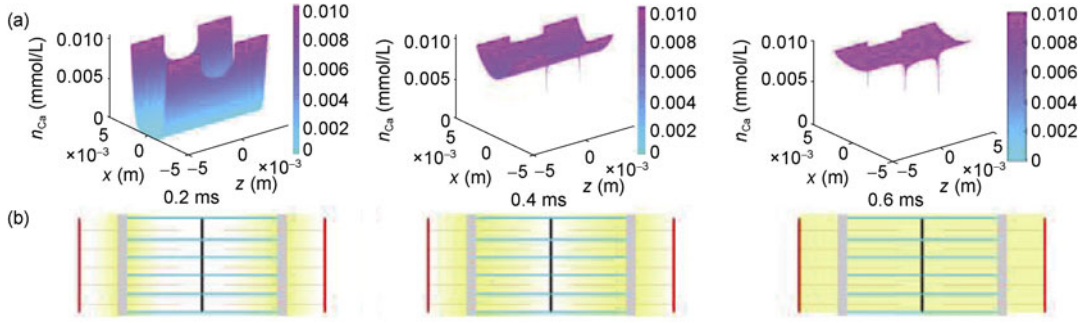

Figure 5 (a) The simulation of $[Ca^{2+}]$ diffusion process in a sarcomere; (b) scheme of the diffusion process.

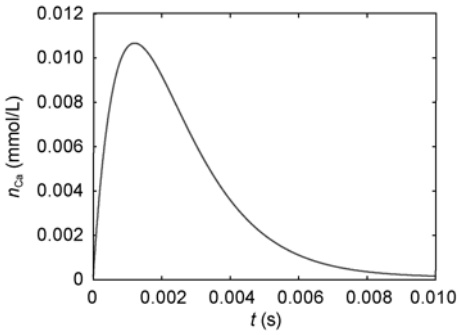

Figure 6 [Ca^{2+}] variation process in a sarcomere during a single action potential.

4 Regulation of [Ca^{2+}] inside sarcomeres by action potential

The so called "all or none" property exists when action potentials burst [24], i.e., their amplitudes are nearly constant and almost do not vary with stimulation intensity. This property holds for the action potentials on sarcolemma, so the [Ca^{2+}] inside sarcomeres can only be modulated via frequency, i.e., the action potentials are variable-frequency control signal. On the other hand, [Ca^{2+}] is directly related to muscle fiber tension, and this is the reason why [Ca^{2+}] is equivalent to the drive signal.

If the frequency of action potentials is very low (e.g., less than 2 Hz), a single sarcomere will exhibit "twitch" behavior, which means that obvious contraction-relaxation cycles appear. When the frequency rises to some extent, the [Ca^{2+}] during unit time becomes uniform, and the originally independent twitches will be so dense as to perform like a constant force. Thus instantaneous [Ca^{2+}] can be approximated by the average [Ca^{2+}] during unit time interval, and this is similar to the conception of equivalent power of alternating current, as shown in Figure 7. Besides, due to the not less than 2.2 ms absolute refractory period of Na^+ channel [25], the maximum frequency of action potentials cannot exceed 450 Hz, and there is almost no intersection among the potentials. It is obvious that the higher the frequency, the higher the temporal mean of [Ca^{2+}]. Such regulation behavior implies that: 1) Under isometric tensions (the two ends of a sarcomere is fixed), the tension provided by the sarcomere is determined by the number of working molecular motors, because the maximum tension a single motor can generate is nearly constant, while the higher the average [Ca^{2+}], the more motors are stimulated, as a result, the larger the tension of the sarcomere. 2) When the load is smaller than the maximum tension a sarcomere can provide, i.e., the sarcomere is able to produce contraction displacement and speed (e.g., isotonic tension), the temporal mean of [Ca^{2+}] actually determines the power of the sarcomere, for the reason that the average [Ca^{2+}] is decided by the number of stimulations of the sarcomere during the unit time (Figure 7).

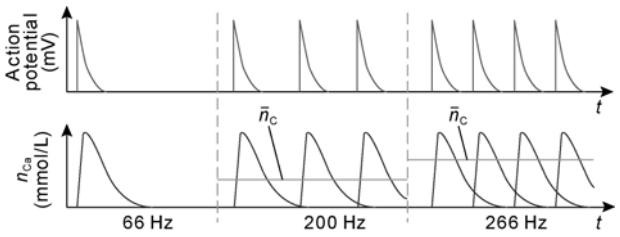

Figure 7 The regulation of [Ca^{2+}] by action potentials.

From the results of eq. (9) and eq. (13), it is not difficult to calculate the relation between frequency of action potentials and average [Ca^{2+}], and actually this can be done via calculating the temporal mean of neighboring [Ca^{2+}] waves in one period. Figure 8(a) shows the simulation result, and the curve obviously exhibits sigmoidal features, indeed, it can be fitted well with the sigmoid function

$$\overline{n_{Ca}} = \frac{a_4}{1+\exp(-b_4 f)} + c_4, \tag{14}$$

where f is the frequency of action potentials, a_4 = 2.009 $\times 10^{-2}$, $b_4 = 7.702\times 10^{-3}$, and $c_4 = -1.008\times 10^{-2}$. As mentioned, the average [Ca^{2+}] determines the amount of stimulated myosin during isometric tension, so it should be positively correlated to the isometric tension, and because of the fixed number of molecular motors in a sarcomere, there should be a saturation value of the contraction force. From the results of the preceding paper [13], the contraction force of muscles can be stated as

$$F = \beta \cdot F_{\max}, \tag{15}$$

where $F_{\max}$ denotes the maximum tension of a muscle, and it is related to the factors such as the cross section area of the muscle, the load, [ATP], etc. The stimulation level of the muscle is characterized by β, which can be expressed as

$$\beta = \frac{[Ca^{2+}]^2}{[Ca^{2+}]^2 + K_2[Ca^{2+}] + K_1 K_2}, \tag{16}$$

where K_1 and K_2 denote the ratios of the separation rate to the binding rate of Ca^{2+} during two stages, and their values are 8.72 and 0.194 μM [26], respectively. Combining eq. (14) and eq. (16), it is easy to obtain the relation between muscle tension and the frequency of action potentials, as shown in Figure 8(b). Note that the tension in Figure 8(b) is expressed as normalized force ($F/F_{\max}$). On the other hand, relevant experiments indeed showed that the relation shown in Figure 8(b) does exist [27]. If investigating it in detail, we find that the relation between the contraction force F and the frequency f can also be expressed by the sigmoid function, which is consistent with the theoretical results of the previous paper [13] and the experimental results of this paper (see experimental results). Referring to control theory, eqs. (14) and (15) represent two serial links during the drive

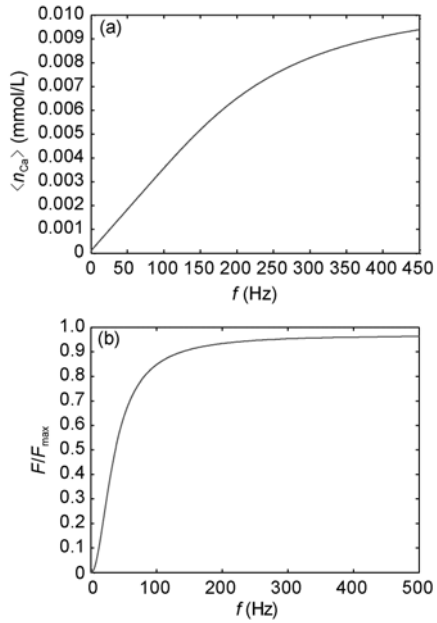

Figure 8 (a) The relation been average $[Ca^{2+}]$ and frequency of action potentials; (b) the relation between normalized tension and frequency of action potentials.

process of muscle fibers. Moreover, we know that many types of skeletal muscles exist [28], and due to the assumption that the K^+ channel density is very high on T-tubules during our modeling, the result shown in Figure 8(a) is closer to the characteristics of fast type muscle fibers, while it may be different to some extent for slow type ones.

Actually the relation in Figure 8(a) is obtained under steady state, i.e., the muscle fiber is stimulated by steady series of action potentials, while for the understanding of the control of muscle contraction, it is equally important to investigate the transient response of the average $[Ca^{2+}]$ to the variation of action potential frequency (e.g., the frequency jumps to 400 Hz from zero), because during the normal operations of muscle, the frequency of action potentials changes all the time, which leads to the variation of muscle power affected by sarcomere $[Ca^{2+}]$. Therefore, the dynamic regulation mode of average $[Ca^{2+}]$ by action potentials is variable-frequency control, and the transfer function from frequency to $[Ca^{2+}]$ can be obtained via system identification as

$$G(s) = \frac{B_1 s^2 + B_2 s + B_3}{s^3 + A_1 s^2 + A_2 s + A_3}, \tag{17}$$

where the coefficients are $B_1 = -0.2794$, $B_2 = -609$, $B_3 = 1.934\times10^5$, $A_1 = 3.887\times10^3$, $A_2 = 9.385\times10^6$, and $A_3 = 8.674\times10^9$. Eq. (17) shows that this is a third-order system, which is apparently composed of an inertia link originated from the chemical diffusion of Ca^{2+} and a second-order vibration link coming from the wave features of action potentials. The system $G(s)$ has two zeros, one positive and the other negative, and three poles whose real parts are negative. Despite of being an open loop system, it is stable against step input and ramp input. From the discussion above, we know that sarcomere $[Ca^{2+}]$ changes frequently when a muscle perform reciprocal motion, and the corresponding frequency of action potentials also varies up and down at this moment, so the frequency domain properties of the system in eq. (17) need to be investigated. The Bode diagram of the system is shown in Figure 9. It should be noted that the physical meaning of the horizontal axis in Figure 9 is "frequency of the frequency", i.e., the variation frequency of the frequency of action potentials, and it corresponds to the variation frequency of sarcomere $[Ca^{2+}]$, which characterizes muscle contraction power. It can be seen from Figure 9 that the amplitudes of the system at low frequencies are almost constant, and reach the maximum at mediate frequencies, while at high frequencies inhibition appears, which is similar to the behavior of a low-pass filter. On the other hand, it has been mentioned that the maximum frequency of action potentials is ~ 450 Hz, thus its variable-frequency must be lower than this value, which is marked by a vertical red line located near the maximum amplitude in Figure 9. This indicates that within the range of variable-frequency, muscle power increases with the frequency of contraction cycles, while it hardly changes at low frequencies. Moreover, the operation frequency domain of muscle fibers does not enter the low-pass filter region.

5 Experimental results

We took experiments on human rectus femoris of thigh to verify the steady relation between the isometric tension of muscle and the frequency of action potentials. Rectus femoris is located at the front of thighs and it connects the tendons of the knee joint and hip joint, thus its contraction will raise the thigh or the leg. The experimental apparatus is shown in Figure 10, and tension signals and EMG signals were collected with the lower limb exoskeleton robot designed by our research group. EMG signals are formed by the superposition of massive action potentials of muscle fibers in a muscle, and the analysis of EMG can be used to

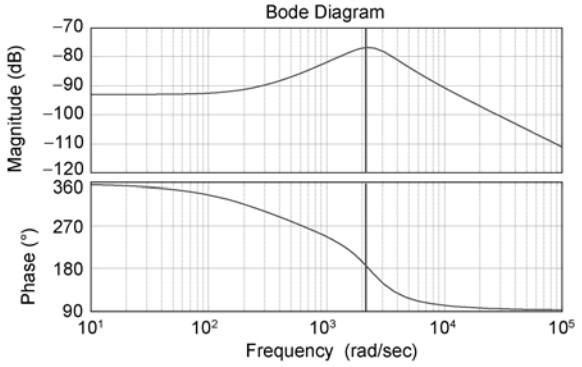

Figure 9 The frequency domain characteristics of the drive signal of muscle fibers.

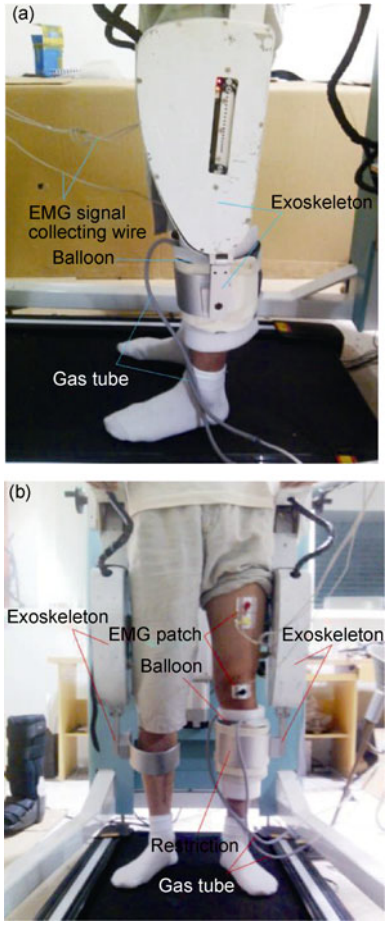

Figure 10 (a) Side view of the experimental apparatus; (b) front view of the experimental apparatus.

diagnose muscle diseases [29] or identify the motion pattern of muscles [30], while here we judged the stimulation level of rectus femoris via the characteristic frequency of EMG.

The exoskeleton has two degrees of freedom, and it can fix the thigh and leg of the experimental subject. During our experiment, the left leg of the subject was bound to the exoskeleton, also bound was his hip joint, so his thigh is not able to move. A balloon used as the pressure transducer connecting with gas tubes was bound to the leg, and both of the balloon and the leg were bound to the exoskeleton by the restriction. EMG patches (electrodes) were located at the middle of rectus femoris to monitor its stimulation level. When the experiment started, the balloon was firstly charged with gas, and then the subject slowly extended his leg out. The rectus femoris contracted during this motion, and its stimulation intensity was recorded by EMG signals. Due to the fixed position of the restriction, actually no displacement of the leg occurred, while the force that the leg exerted on the balloon varied in the process, thus the pressure of the balloon always changed, and the tension of rectus femoris could be characterized by this pressure. Therefore, EMG signals under different contraction conditions of the rectus femoris could be obtained. The sampling rates of EMG signal and tension signal were both 2000 Hz, so one datum was recorded every 400 sampling interval, i.e., the data recording period was $\Delta T = 0.2$ s. In the experiment the EMG signals during every ΔT were dealt with Fourier transform and the characteristic frequency was extracted in real time. The formula of the characteristic frequency is

$$f_{\mathrm{ch}} = \frac{\sum_{i=1}^{N} A_i n_i}{\sum_{i=1}^{N} A_i} \cdot \xi, \tag{18}$$

where A_i denotes the amplitudes of the points on the half Fourier spectrum, n_i is the position of the point, and N denotes total number of sampling points. For the reason that the ranges of EMG frequency and action potential frequency of a single muscle fiber are different, an adjustment coefficient ξ was introduced, and it matched the experimental EMG frequency with the action potential frequency of muscle fibers so as to better verify the relation between tension and action potential frequency. As mentioned, the frequency range of action potentials is ~ 450 Hz, while the range of EMG frequencies in the experiment was ~ 60 Hz, so we took $\xi = 1/8$. The characteristic frequency f_{ch} was also output in real time, as well as the mean force during ΔT.

One group of original data of balloon pressure and f_{ch} of EMG are shown in Figure 11(a), from which we see that

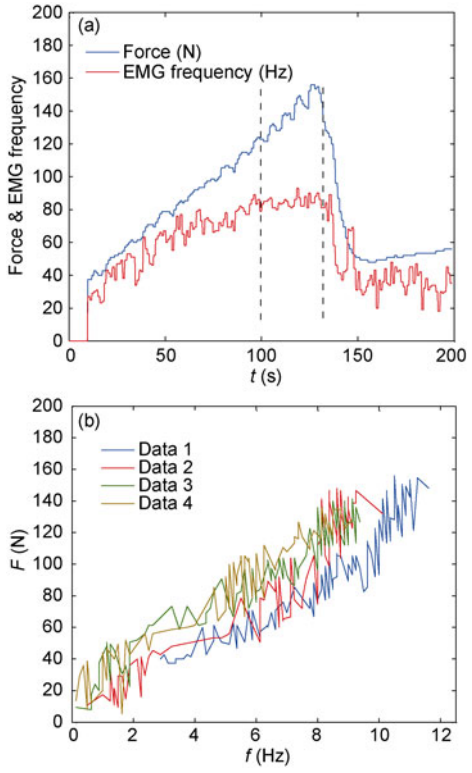

Figure 11 (a) Real-time data of pressure and EMG frequency; (b) four successive groups of experimental data.

these two quantities approximately follow each other, i.e., the higher the EMG frequency, the larger the force (the tension of rectus femoris). Note that when f_{ch} reaches the peak value and does not change with time (the region between the dashed lines in Figure 11(a)), the force remains growing for a while. This is because the number of stimulated muscle fibers is increasing under the same stimulation level. Figure 11(b) shows four groups of successively processed experimental data, which have already been expressed as the relation between the pressure and EMG frequency. The subject had a rest of 4–5 min between groups, still it is obvious that the contraction force at the same frequency became larger in later sets of data, i.e., the number of muscle fibers stimulated by action potentials of the same frequency would increase. This phenomenon is called "activity-dependent potentiation" [31], after which fatigue happens.

To avoid the effect of fatigue, we fitted the data in the first and the second groups in Figure 11(b). The experimental data and the fitted curve are shown in Figure 12(a), and the fitting process is based on the sigmoidal feature of the data. The resulted function writes

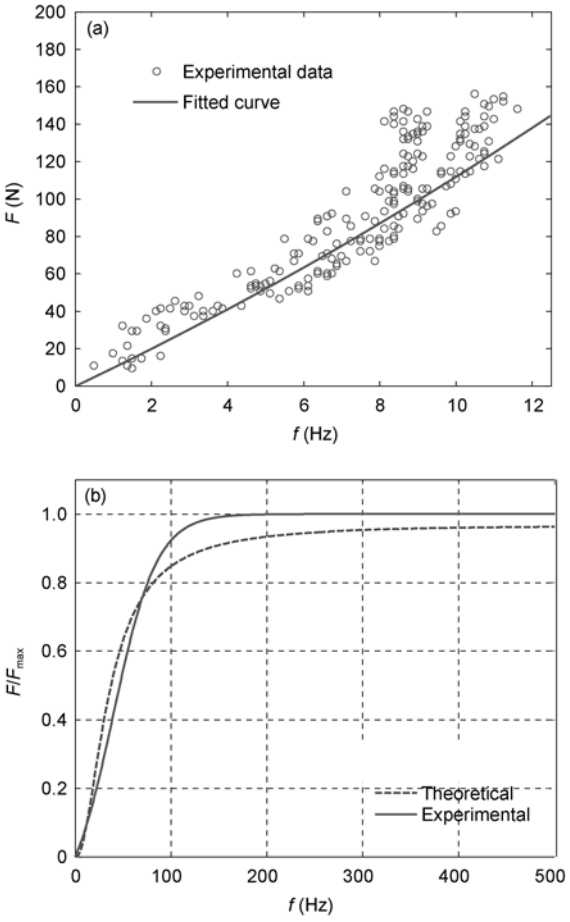

Figure 12 (a) The fitted curve of the experimental data; (b) comparison between the experimental and theoretical curves.

$$F = \frac{a_5}{1+\exp(-b_5(f+c_5))} + d_5, \tag{19}$$

where F and f are the pressure and the EMG frequency, respectively. The parameters are $a_5 = 1734$, $b_5 = 5.503 \times 10^{-3}$, $c_5 = -318$, and $d_5 = -256.724$. The fitted curve represents the realistic steady relation between muscle contraction force and action potential frequency, and Figure 12(b) compares the normalized experimental relation expressed in eq. (19) with the theoretical relation (Figure 8(b)). From the figure we see that the changing trend of the theoretical curve is basically consistent with that of the experimental one, and that the slopes of the curves match during the stage of the normalized force increasing with the frequency, while the theoretical curve falls behind the experimental one near the saturation stage, and after that the experimental curve always leads. This is due to the slow approaching to infinity process of the force reaching the maximum value, according to the theoretical results. On the other hand, Hill and Kesar et al. measured the muscle forces of the subjects *in vivo* with the method of functional electric stimulation (FES) [32, 33]. Their researches aimed at the fatigue process of human muscles, and the frequency of FES was able to reach 100 Hz. On the contrary, in our experiment the subject provided force actively while EMG frequency was measured. Although the input and output were reversed in these two kinds of experiments, the corresponding relation should hold, and indeed, such consistence is also shown in Figure 12(b).

6 Discussion

This paper started from the geometric and physiologic features of sarcomeres, then provided the physical model for action potentials and $[Ca^{2+}]$ variation in a half sarcomere. Finally, the mechanism of action potentials (the control signal) regulating $[Ca^{2+}]$ (the drive signal) was obtained. When discussing $[Ca^{2+}]$, we calculated the time τ_c for it to reach the peak value, and this time interval is regarded as a characteristic constant and holds special significance, because it represents the minimum time for muscle fibers to contract after the control signal happens. This time constant is similar to the electromechanic time constant in mechatronic control and is decided by the physical properties of muscle fibers. For the reason that τ_c is the time constant of skeletal muscle and action potentials are electric signals, we name it as "electro-muscular time constant", without losing representativeness. When elucidating how $[Ca^{2+}]$ is controlled by action potentials, we proposed two indications of the regulation mechanism, which plays a key role in the understanding of motion intention. From the indications we know that although the final representation of motion intention is muscle force (contraction speed and displace-

ment are also dominated by the force), motion intention cannot be quantified by measuring the contraction force. This is because when the same action potentials are applied to different motor units, the tension and power produced can differ a lot due to the different numbers of sarcomeres/ myosins contained in them. Therefore, the frequency of action potentials actually represents "intention strength", while the contraction force represents "action strength". Of course the intention strengths for different muscles/people should be different in order to generate the same action strengths. On the other hand, this paper deduced the theoretical steady relation between action potential frequency and muscle force, and we further designed the corresponding experiment to verify the theoretical results. The results show that the experiment well coincides with the theory.

This paper further elucidated the regulation mode of average $[Ca^{2+}]$ in sarcomeres by action potential-variable-frequency modulation, and derived the dynamic response of $[Ca^{2+}]$ to the variation of action potential frequency, with the transfer function provided. Besides, with the frequency domain analysis of the resulted system, we found that the power will gradually increase from the initially constant value with the rise of contraction frequency of muscle fibers, i.e., for some type of skeletal muscle, there exists a contraction frequency at which its power is at maximum, and this frequency is decided by both the highest frequency of action potentials and frequency domain characteristics of muscle contraction. There also exists the upper limit of contraction frequency of muscle fibers, while it is only decided by the maximum frequency of action potentials.

If combining the concept of electro-muscular time constant with the regulation and control mechanism of sarcomere contraction, it is not difficult to tell that the theoretical results of this paper actually provide the first forward transfer function of skeletal muscle control links, although deduced with the sarcomere closest to the sarcolemma. Thus based on these results the control characteristics of a muscle fiber can be obtained with the distributions of action potentials and sarcomeres. Furthermore, the control model of the whole muscle can also be obtained because a single piece of muscle is composed of massive muscle fibers in series and in parallel, then the unification of microscopic and macroscopic models for skeletal muscles can be completed. While this paper has provided the regulation mechanism and properties of sarcomere contraction, it does not mean that the whole control model has formed because the real muscle operation process is in a closed-loop system fed back via biologic neural network. In this paper only the open-loop characteristics of muscle fibers were discussed, thus in future studies, the information feedback features of skeletal muscle motion should be further explored based on the mechanism presented here. Finally the complete transfer function of skeletal muscle control can be obtained.

This work was supported by the National Natural Science Foundation of China (Grant No. 61075101), the Research Fund of State Key Laboratory of MSV, China (Grant No. MSV-2010-01), the Medical and Technology Intercrossing Research Foundation (Grant No. YG2010ZD101), and the Science and Technology Intercrossing Research Foundation of Shanghai Jiaotong University.

1 Hill A V. The heat of shortening and the dynamic constants of muscle. Proc R Soc Lond B, 1938, 126: 136–195
2 Gordon A M, Huxley A F, Julian F J. The variation in isometric tension with sarcomere length in vertebrate muscle fibres. J Physiol, 1966, 184: 170–192
3 Ai B Q, Wang X J, Liu G T, et al. Dynamic model for muscle's motion (in Chinese). ACTA Sci Nat Univ Sunyatseni, 2001, 40(6): 27–30
4 Telley I A, Denoth J, Stussi E, et al. Half-sarcomere dynamics in myofibrils during activation and relaxation studied by tracking fluorescent markers. Biophys J, 2006, 90: 514–530
5 Yin Y H, Guo Z. Collective mechanism of molecular motors and a dynamic mechanical model for sarcomere. Sci China Tech Sci, 2011, 54(8): 2130–2137
6 Huxley H E. The mechanism of muscular contraction. Science, 1969, 164: 1356–1366
7 Huxley A F. Muscular contraction. J Physiol, 1974, 243: 1–43
8 Huxley A F, Simmons R M. Proposed mechanism of force generation in striated muscle. Nature, 1971, 233: 533–538
9 Spudich J A. How molecular motors work. Nature, 1994, 372: 515–518
10 Anthony L F, Erickson H P, Rousseau E, et al. Purification and reconstitution of the calcium release channel from skeletal muscle. Nature, 1988, 331: 315–319
11 Cannel M B, Allen D G. Model of calcium movements during activation in the sarcomere of frog skeletal muscle. Biophys J, 1984, 45: 913–925
12 Stuyvers B D, McCulloch A D, Guo J Q, et al. Effect of simulation rate, sarcomere length and Ca^{2+} on force generation by mouse cardiac muscle. J Physiol, 2002, 544, 3: 817–830
13 Guo Z, Yin Y H. A dynamic model of skeletal muscle based on col-lective behavior of myosin motors—Biomechanics of skeletal muscle based on working mechanism of myosin motors (I). Sci China Tech Sci, 2012, 55:
14 Jayasinghe I D, Cannell M B, Soeller C. Organization of ryanodine receptors, transverse tubules, and sodium-calcium exchanger in rat myocytes. Biophys J, 2009, 97(10): 2664–2673
15 Tanabe T, Takeshima H, Mikami A, et al. Primary structure of the receptor for calcium channel blockers from skeletal muscle. Nature, 1987, 328: 313–318
16 Takeshima H, Nishimura S, Matsumoto T, et al. Primary structure and expression from complementary DNA of skeletal muscle ryanodine receptor. Nature, 1989, 339: 439–445
17 Toyoshima C, Nakasako M, Nomura H, et al. Crystal structure of the calcium pump of sarcoplasmic reticulum at 2.6 Å resolution. Nature, 2000, 405: 647–655
18 Fortune E, Lowery M M. Effect of extracellular potassium accumulation on muscle fiber conduction velocity: A simulation study. Ann Biomed Eng, 2009, 37(10): 2105–2117

19 Piitulainen H, Botter A, Merletti R, et al. Muscle fiber conduction velocity is more affected after eccentric than concentric exercise. Euro J App Physiol, 2010, 111(2): 261–273

20 Maxwell M H, Kleeman C R. Clinical Disorders of Fluid and Electrolyte Metabolism. New York: McGraw-Hill Companies, 1968. 28

21 Endo M. Calcium-induced calcium release in skeletal muscle. Physiol Rev, 2009, 89: 1153–1176

22 Escobar A L, Monck J R, Fernandez J M, et al. Localization of the site of Ca^{2+} release at the level of a single sarcomere in skeletal muscle fibres. Nature, 1994, 367: 739–741

23 Dux L, Martonosi A. Two-dimensional arrays of proteins in sarcoplasmic reticulum and purified Ca^{2+}-ATPase vesicles treated with vanadate. J Biol Chem, 1983, 258: 2599–2603

24 Levitan I B, Kaczmarek L K. The Neuron Cell and Molecular Biology. 2nd ed. New York: Oxford University Press Inc, 1997. 37–39

25 Allen D C, Arunachalam R, Mills K R. Critical illness myopathy: Further evidence from muscle-fiber excitability studies of an acquired channelopathy. Muscle Nerve, 2008, 37: 14–22

26 Baylor S M, Hollingworth S. Calcium indicators and calcium signalling in skeletal muscle fibres during excitation-contraction coupling. Prog Biophys Mol Biol, 2011, 105: 162–179

27 Kreutziger K L, Piroddi N, Scellini B, et al. Thin filament Ca^{2+} binding properties and regulatory unit interactions alter kinetics of tension development and relaxation in rabbit skeletal muscle. J Physiol, 2008, 586, 15: 3683–3700

28 MacIntosh B R, Gardiner P F, McComas A J. Skeletal Muscle: Form and Function. 4th ed. Xi'an: Fourth Millitary Medical University Press, 2010. 4–5

29 Chen Z R. Clinical application of electromyography (EMG). J Mod Electrophysiol, 2005, 12(1): 42–46

30 Wang F, Luo Z Z. Based on the power-spectrum to classify the pattern of the surface electromyography. J Hangzhou Inst Electr Eng, 2005, 25(2): 37–40

31 Pasquet B, Carpentier A, Duchateau J, et al. Muscle fatigue during concentric and eccentric contractions. Muscle Nerve, 2000, 23: 1727–1735

32 Edwards R H T, Hill D K, Jones D A, et al. Fatigue of long duration in human skeletal muscle after exercise. J Physiol, 1977, 272: 769–778

33 Kesar T, Chou L W, Binder-Macleod S A. Effects of stimulation frequency versus pulse duration modulation on muscle fatigue. J Electromyogr Kinesiol, 2008, 18(4): 662–671